LiZnSO₄F Made in an Ionic Liquid: A Ceramic Electrolyte Composite for Solid-State Lithium Batteries

Prabeer Barpanda, Jean-Noël Chotard, Charles Delacourt, Marine Reynaud, Yaroslav Filinchuk, Michel Armand, Michael Deschamps, and Jean-Marie Tarascon*

The search for good solid electrolytes constitutes a major goal towards the development of safer lithium batteries. A few candidates do exist, but they suffer either from narrow electrochemical window stability or too low ionic conductivity. Herein we report the ionic-liquid-assisted synthesis of a novel $LiZnSO_4F$ fluorosulfate phase having a sillimanite $LiTiOPO_4$-type structure, which on simply pressed samples shows a room-temperature ionic conductivity of 10^{-5}–$10^{-7}\,S\,cm^{-1}$ together with a 0–5 V electrochemical stability window range, while ionic-liquid-free $LiZnSO_4F$ shows an ionic conductivity four orders of magnitude lower ($10^{-11}\,S\,cm^{-1}$). While robustly reproducible but not yet fully understood, this finding offers new opportunities to tailor inorganic composites with higher ionic conductivity. The origin of such results is demonstrated to be rooted in a surface effect associated with the grafting of a lithium-containing ionic liquid layer. This finding opens up new opportunities for the design of ceramic composites with higher ionic conductivity and should serve as an impetus for further exploiting the chemistry of ionic liquid grafting on oxides.

Renewable energy sources and electric automotive transportation are popular topics in today's energy-conscious society, hence placing rechargeable batteries as one of the major technological sciences in this new century.[1] Advances in energy storage are a tribute to chemists' abilities to design new and better materials. In the hunt for novel electrode materials, notions of sustainability must be considered.[2] This is the reason why $LiFePO_4$, which is made of inexpensive and abundant chemical elements, has attracted the attention of the research community despite its poor conducting properties. By particle downsizing and carbon nanocoating, $LiFePO_4/C$ composite overcomes transport limitations and is capable of reversibly and rapidly intercalating 0.9 Li

(ca. $160\,mA\,h\,g^{-1}$) at a redox voltage of 3.43 V versus Li. Thus, it has become one of the most praised electrode materials for the next generation of rechargeable batteries for high-volume applications.[3]

Further exploring the chemistry of polyanionic-based insertion electrodes, we recently synthesized, by an ionothermal process, a novel 3.6 V $LiFeSO_4F$ electrode showing a reversible capacity nearing $140\,mA\,h\,g^{-1}$ (theoretical capacity = $151\,mA\,h\,g^{-1}$), good rate capability, and cycling stability.[4] This fluorosulfate was found to crystallize in a tavorite structure (space group $P\bar{1}$) with three-dimensional channels for Li diffusion as opposed to the one-dimensional channels in $LiFePO_4$. Most likely, from the 3D versus 1D change in the conduction path, the use of $LiFeSO_4F$ powders will obviate the need for nanosizing or carbon coating, while the same cost and environmental advantages are maintained.

Since our early report, we have considerably enlarged the fluorosulfate family with the discovery of $AMSO_4F$ (A = Li, Na and M = Co, Ni, Mn, etc.) homologues.[5] This new family of materials, practically unknown a year ago, counts no less than 20 members showing related structures with either promising electrochemical or attractive ionic properties. Among them, the sodium-based 3d-metal fluorosulfates, which crystallize in a titanite structure (derived from the tavorite structure, space group $P2_1/c$) and have localized positions for the Na^+ ions, were found to show a four-fold increase in ionic conductivity as compared to their Li-based counterparts on cold-pressed powders ($10^{-7}\,S\,cm^{-1}$ for Na vs. $10^{-11}\,S\,cm^{-1}$ for Li at room temperature). While far from the hallmark solid-state electrolytes for future Li batteries such as $Li_{1.5}Al_{0.5}Ge_{1.5}(PO_4)_3$ (LAG), $Li_{1.3}Al_{0.3}Ti_{1.7}(PO_4)_3$ (LAT), and $Li_{3+x}PO_{4-x}N_x$ (LIPON), which have room-temperature conductivities of $2.8 \times 10^{-4}\,S\,cm^{-1}$, $10^{-3}\,S\,cm^{-1}$, and $10^{-6}\,S\,cm^{-1}$, respectively, such a finding was an impetus to look for further fluorosulfate members as part of the effort to develop new ceramic electrolyte materials with increased conductivity, thus allowing a switch from thin-film to bulk technology in all solid-state batteries.[6]

Besides high ionic conductivity, a pivotal figure of merit for solid-state electrolytes is the width of their electrochemical stability window. This window is limited for ionic conducting ceramics containing 3d-metal elements, such as $Li_{1.3}Al_{0.3}Ti_{1.7}(PO_4)_3$, owing to the reduction of Ti^{4+} in Ti^{3+} at approximately 2.4 V. So our strategy was to search for other members of the fluorosulfate $AMSO_4F$ family containing divalent metals that cannot be easily reduced or oxidized. Besides $LiMgSO_4F$, the first reported fluorosulfate,[7] other attractive candidates could enlist lead, tin, or zinc to prepare $AMSO_4F$ phases. Mindful of the previously reported struc-

[*] Dr. P. Barpanda, Dr. J.-N. Chotard, Dr. C. Delacourt, M. Reynaud, Prof. M. Armand, Prof. J.-M. Tarascon
Laboratoire de Réactivité et Chimie des Solides
Université de Picardie Jules Verne, CNRS UMR 6007
33, rue Saint Leu, 80039 Amiens (France)
E-mail: jean-marie.tarascon@sc.u-picardie.fr
Homepage: http://jmtarascon.tech.officelive.com

Dr. Y. Filinchuk
Swiss–Norwegian Beamlines at ESRF, BP-220
6, rue Jules Horowitz, 38043 Grenoble (France)

Dr. M. Deschamps
Centre de Recherches sur les Matériaux à Hautes Températures
CNRS UPR 4212, 1D avenue de la Recherche Scientifique, 45071
Orléans (France)

2526 WILEY ONLINE LIBRARY

© 2011 Wiley-VCH Verlag GmbH & Co. KGaA, Weinheim

Angew. Chem. Int. Ed. **2011**, 50, 2526–2531

tural affiliation between the precursor $MSO_4 \cdot H_2O$ and the product $AMSO_4F$ phase, we searched for $MSO_4 \cdot H_2O$ phases (M = Zn, Pb, and Sn) having the same structure as $FeSO_4 \cdot H_2O$. We identified $ZnSO_4 \cdot H_2O$ to be isostructural with $FeSO_4 \cdot H_2O$. Thus, we prepared the $ZnSO_4 \cdot H_2O$ precursor either by using the ionic liquid (IL) 1-ethyl-3-methylimidazolium bis(trifluoromethanesulfonyl)imide (EMI-TFSI) or by a ceramic route and later treated it with a stoichiometric amount of LiF at 300°C by either ionothermal or solid-state (ceramic) synthesis. We succeeded in preparing the $LiZnSO_4F$ phase involving a topotactic reaction; the structural and transport properties of this phase are reported. Depending upon the IL or ceramic-based precursors, the final products are henceforth named $LiZnSO_4F$-IL or $LiZnSO_4F$-C, respectively. We found that $LiZnSO_4F$ does not crystallize into a tavorite (triclinic) structure but instead favors a sillimanite (orthorhombic) structure and shows a room-temperature ionic conductivity of 10^{-5}–10^{-7} S cm^{-1}.

The crystal structure of $LiZnSO_4F$ was solved from synchrotron data by Rietveld refinement using the FullProf program.[8] Isostructural with the sillimanite $LiTiOPO_4$ structure (Figure 1a),[9] $LiZnSO_4F$ crystallizes into an orthorhombic cell (space group: *Pnma*) with the cell parameters $a = 7.40357(9)$ Å, $b = 6.32995(7)$ Å, $c = 7.42016(9)$ Å and $V = 347.740(7)$ Å^3. All crystallographic data as well as agreement factors are summarized in Table 1 (corrected for background). The high χ^2 value mainly reflects the extremely high counting statistics of the powder diffraction data obtained from a 2D detector. The structure (Figure 1b) is built up from SO_4 tetrahedra and zinc-centered ZnO_4F_2 octahedra. The latter are linked together through fluorine atoms (in *trans* positions), thus creating chains along the *a* axis. These chains are interconnected by SO_4 tetrahedra. Indeed, each SO_4 tetrahedron shares two of its vertices with two ZnO_4F_2 octahedra from a first chain, while the two remaining vertices are linked to two other ZnO_4F_2 chains (see the Supporting Information). This arrangement leads to the formation of tunnels along the *a* axis (Figure 1b) that host Li atoms.

The ionic conductivity was measured with ionically blocking electrodes for $LiZnSO_4F$-IL pressed pellets. Typical impedance spectra (a small semicircle along with a large Warburg diffusion tail) suggest a very high ionic mobility. Ionic conductivity values as high as 2.8×10^{-5} S cm^{-1} were repeatedly recorded at room temperature for several samples (Figure 2a); these values were six orders of magnitude higher than for the tavorite $LiFeSO_4F$ compound. This manifold increase in conductivity can be due either to the crystal structure or to the surface modification in $LiZnSO_4F$ (e.g. onset of grain boundaries).

Taking advantage of the non-paramagnetic Zn center, we performed a solid-state NMR spectroscopy (^{19}F, ^1H, and ^7Li) study, which captured the narrow ^1H and ^{19}F signals arising from the EMI-TFSI ionic liquid (Figure 3). The ^1H NMR spectrum of $LiZnSO_4F$-IL features the five peaks characteristic of the EMI cation. Moreover, their positions are shifted by $\delta = -1.5$ ppm (Figure 3c) as compared to free EMI-TFSI, probably because of the change in magnetic susceptibility at the $LiZnSO_4F$-IL surface.[10] Besides, the ^{19}F NMR spectrum
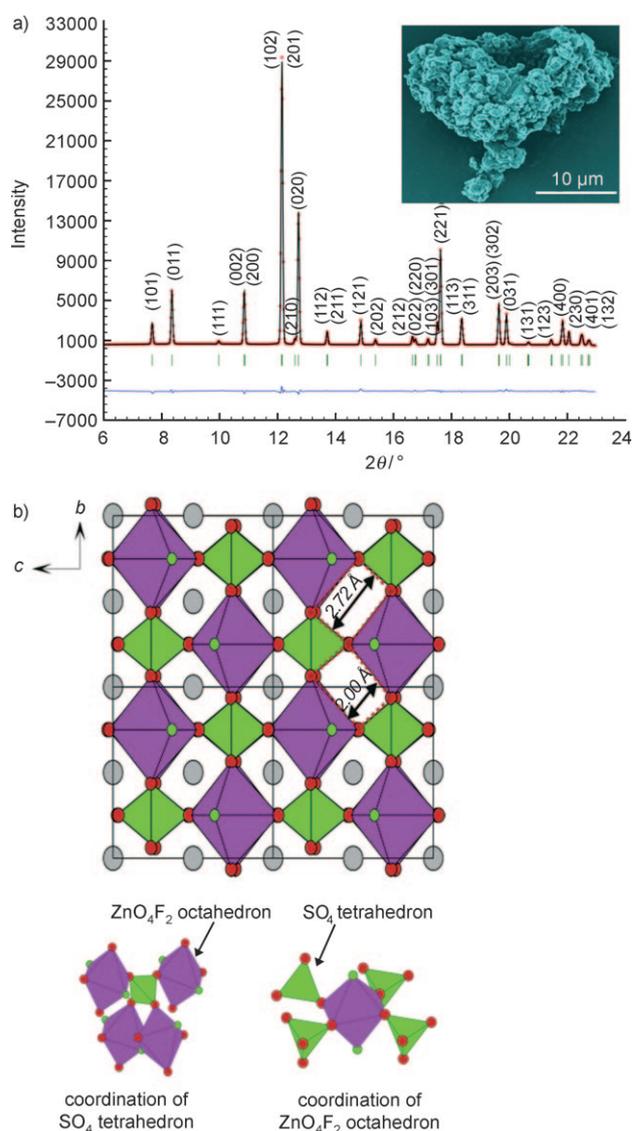
Figure 1. a) Synchrotron XRD pattern ($\lambda = 0.701277$ Å) of single-phase $LiZnSO_4F$. The red dots are the experimental diffraction pattern, the black line is the simulated pattern, the green ticks are the Bragg peak positions, and the blue line is the difference between the experimental and the simulated pattern. The inset shows a representative SEM image with a particle size range of 800–1200 nm. b) The sillimanite structure of $LiZnSO_4F$ showing the interconnected ZnO_4F_2 octahedra (pink), SO_4 tetrahedra (green), and Li atoms. Li gray, O red, F green. The local coordination of a SO_4 tetrahedron and a ZnO_4F_2 octahedron is also shown. Further structural images are shown in the Supporting Information.

reveals three distinct signals, one narrow (e.g. mobile) signal corresponding to the trifluoromethyl groups from TFSI, another broader, intense signal from F within the crystallized $LiZnSO_4F$ structure, and the third corresponding to F from LiF. Interestingly, the ^{19}F signals coming from the IL and LiF are amplitude-correlated. From these NMR spectroscopy measurements, we estimate the ionic liquid monolayer trapped at the surface of the $LiZnSO_4F$ particles to range from 8–15 nm, assuming particles having an average diameter of 0.5–1 μm. The presence of ionic liquid in the final samples

Table 1: Lattice parameters, cell volume, and atomic coordinates for LiZnSO$_4$F with orthorhombic (*Pnma*) symmetry.

LiZnSO$_4$F	a [Å]	b [Å]	c [Å]	Volume [Å^3]
	7.40357(9)	6.32995(7)	7.42016(9)	347.740(7)
	α	β	γ	
	90°	90°	90°	
	χ^2	R_p	R_{wp}	R_{Bragg}
	1730	3.26	3.48	0.88

Atom	Wyckoff position	x	y	z
Li	4a	0	0	0
Zn	4c	0.14345(18)	$^1/_4$	0.29262(14)
F	4c	0.4011(7)	$^1/_4$	0.3660(3)
S	4c	0.3623(4)	$^1/_4$	0.8589(3)
O1	8d	0.1270(5)	0.5625(4)	0.2352(3)
O2	4c	0.2033(7)	$^1/_4$	−0.0239(5)
O3	4c	0.0298(8)	$^1/_4$	0.5380(5)

was also assessed by FTIR spectroscopy and X-ray photoelectron spectroscopy (XPS, see the Supporting Information). Traces of ionic liquid come from the IL-assisted synthesis of the ZnSO$_4$·H$_2$O precursor, which can modify LiZnSO$_4$F grain boundaries by surface coating and consequently affects its ionic conductivity.

To check this assumption, we washed the ZnSO$_4$·H$_2$O precursor with ethyl acetate several times to remove any IL contamination. Consequently, the ionic conductivity dropped to approximately 10^{-7} S cm^{-1} at room temperature after two thorough washing steps and remained constant whatever the number of subsequent washings (Figure 2a). Furthermore, we prepared LiZnSO$_4$F-C products from an ionic-liquid-free ZnSO$_4$·H$_2$O precursor (e.g. obtained from a vacuum temperature-driven process). This material bears the same X-ray pattern and crystal structure as those made by the IL route and, as expected, its ^{19}F NMR spectra does not show any peaks corresponding to TFSI (Figure 3). It exhibits an ionic conductivity of approximately 10^{-11} S cm^{-1}, which is similar to the conductivity of the parent LiFeSO$_4$F fluorosulfate phase. Interestingly, the ionic conductivity of the LiZnSO$_4$F-IL samples remains the same (ca. 10^{-7} S cm^{-1}) whatever the number of washing steps in ethyl acetate, implying that 1) the LiZnSO$_4$F-IL grains are covered with an ionic liquid layer strongly interacting with the grain surface and 2) the ionic liquid "contamination" of the precursor ZnSO$_4$·H$_2$O phase is crucial in controlling the ionic conductivity of the LiZnSO$_4$F-IL compounds. Last, it should be mentioned that annealing the LiZnSO$_4$F-C in ionic liquid at 280°C for 24 h does not affect its ionic conductivity (ca. 10^{-11} S cm^{-1}). For each reported data value, measurements were repeated three times, and inherent errors were small ($\pm 0.3 \times 10^{-6}$ S cm^{-1}), giving us confidence that our observed trends are robust.

DC polarization measurements on ionic-liquid as well as ceramic-precursor-based LiZnSO$_4$F were performed on symmetric Li | PEO-LiClO$_4$ | LiZnSO$_4$F | PEO-LiClO$_4$ | Li cells at 70°C. The possibility of measuring currents (Figure 2b) implies first the existence of Li$^+$ mobility within LiZnSO$_4$F. Secondly, the markedly higher current measured for LiZnSO$_4$F-IL than for LiZnSO$_4$F-C is fully consistent with our
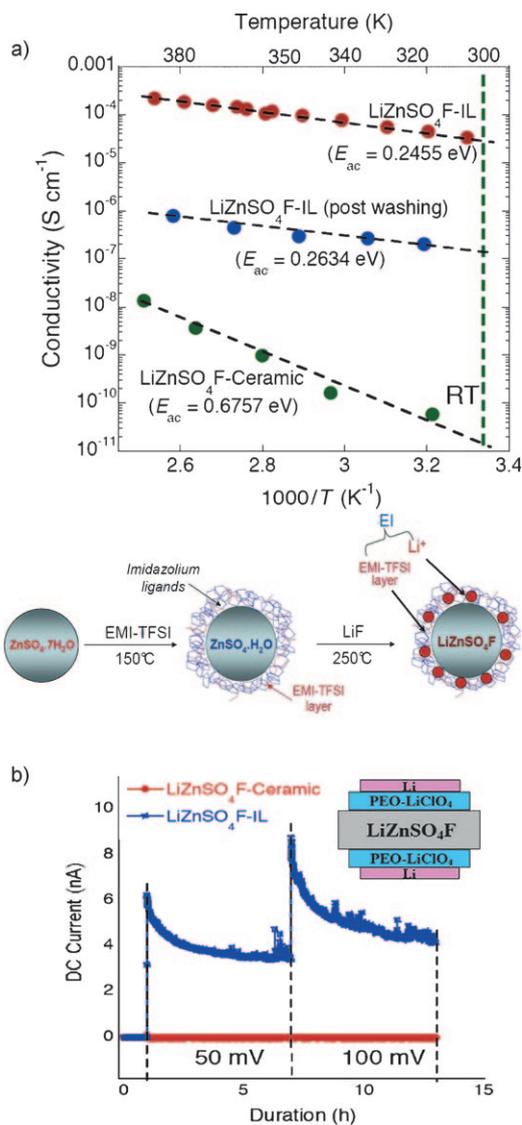
Figure 2. a) AC conductivity of ionically blocking LiZnSO$_4$F pellets prepared using ZnSO$_4$·H$_2$O precursor made with and without ionic liquid. The presence of a thin layer of ionic liquid (from the precursor) leads to a very high Li-ion room-temperature conductivity of approximately 10^{-5} S cm^{-1}. Even after multiple washings of the sample with ethyl acetate, a permanent layer of ionic liquid remains on LiZnSO$_4$F, giving a high conductivity of about 10^{-7} S cm^{-1}. A schematic depiction of the ionic conductivity enhancement caused by the capture of ionic liquid layer around the particles is given (bottom). The "ceramic" LiZnSO$_4$F sample, on the other hand, gives a very low conductivity of approximately 10^{-11} S cm^{-1}. The activation energy values (E_{ac}) are provided. b) Polarization current measurement of LiZnSO$_4$F pellets with and without ionic liquid in a Swagelok cell with Li | PEO | LiZnSO$_4$F | PEO | Li configuration (inset; PEO = poly(ethylene oxide)). The current solely involves Li$^+$ ion mobility through the LiZnSO$_4$F pellet, thus showing that it is a Li$^+$ ion conductor. The presence of ionic liquid favors higher Li$^+$ ion conductivity.

conductivity measurements, which reveal the same trend. The steady-state current at times beyond the establishment of a concentration gradient in the PEO films with this setup is related to the lithium-ion conductivity. Indeed, the Li | PEO-LiClO$_4$ interface is only reversible for lithium (in the absence
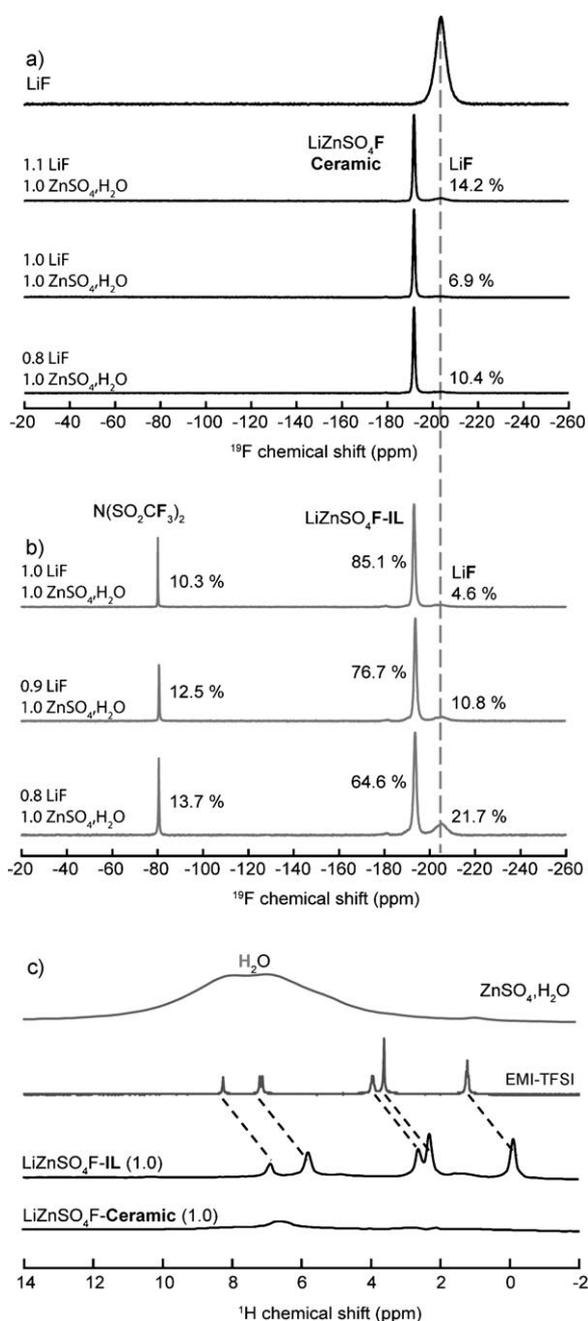
Figure 3. a) ^{19}F NMR spectra of LiF and LiZnSO$_4$F ceramic prepared with 1.1, 1.0, and 0.8 mol of LiF per 1.0 mol ZnSO$_4$·H$_2$O. b) ^{19}F NMR spectra of LiZnSO$_4$F-IL samples with different LiF/ZnSO$_4$·H$_2$O ratios, featuring an additional peak corresponding to the CF$_3$ group of TFSI at $\delta = -80$ ppm. c) ^{1}H NMR spectrum of IL-free ZnSO$_4$·H$_2$O and pure EMI-TFSI compared with LiZnSO$_4$F-IL showing a $\delta = -1.5$ ppm shift between the two spectra, and LiZnSO$_4$F ceramic.

of any side reaction), and PEO-LiClO$_4$ is an electronic insulator.

Both impedance and DC polarization measurements jointly confirm a greater ionic conductivity for the ionic-liquid-made LiZnSO$_4$F samples as compared to the ceramic ones and by the same token highlight the positive role of the ionic liquid treatment in improving the ionic conductivity of

LiZnSO$_4$F. At first, we might hypothesize that such an ionic conductivity results from an encapsulation of the LiZnSO$_4$F grains by a layer of ionic liquid that provides the proper percolation network for ionic conduction. Nevertheless, it remains crucial to understand the underlying mechanism underpinning such a finding.

We should recall that ionic liquids are good ionic conductors, with conductivities of approximately 10^{-2} S cm^{-1} for EMI-TFSI. So the high ionic conductivities (ca. 10^{-5}–10^{-7} cm^{-1} s) measured for LiZnSO$_4$F-IL samples could simply be due to the ionic liquid layers forming a percolating path around the LiZnSO$_4$F. Such a picture, however, is not correct, as it does not take into account the DC polarization measurements, which imply a Li$^+$ ionic conduction. Moreover, we have shown that $\log\sigma = f(1/T)$ for LiZnSO$_4$F nicely follows an Arrhenius law, thus implying that the measured ionic conductivity is not dictated entirely by the ionic liquid, as the temperature dependence of ionic conductivity for the latter follows a Vogel–Tamman–Fulcher (VTF) law. However, the above AC and DC measurements can be reconciled by assuming that the ionic liquid layers will solvate Li$^+$ ions; this hypothesis is well supported by the existence of 1M LiX solutions in EMI-TFSI electrolytes (X$^-$ = PF$_6^-$, TFSI$^-$, etc.). The TFSI anion, though weakly coordinating, is able to solvate lithium.[11] So the observed IL-driven ionic conductivity increase for the LiZnSO$_4$F-IL samples is most likely due to a Li-bearing ionic liquid layer grafted onto the surface of the LiZnSO$_4$F particles (Figure 2a). Such a surface effect does not come as a total surprise as there is past and recent evidence showing the feasibility 1) of apparently enhancing bulk conductivity by creating fast ion-conduction surfaces through controlled adjustment of stoichiometry[12] or 2) of using hybrid ionic-liquid-tethered nanoparticle materials doped with LiTFSI as electrolytes for Li batteries.[13,14] It now remains to be explained by which process some ionic liquid layers remain trapped at the surface of the particle and how they could affect the resulting sample ionic conductivity.

Our synthesis experiments clearly imply that the ionic liquid capturing step occurs during the formation of ZnSO$_4$·H$_2$O precursor from ZnSO$_4$·7H$_2$O in ionic liquid medium, as LiZnSO$_4$F ceramic samples annealed at 280°C in ionic liquid were shown (as deduced from IR measurements) to be IL-free. Such a dehydration process, which involves the departure of water in a hydrophobic ionic liquid medium, leads to an interfacial H$_2$O/ionic liquid medium which, by virtue of a yet unknown mechanism, leads to the fixation of an ionic liquid layer at the surface of the ZnSO$_4$·H$_2$O material. The reaction of ZnSO$_4$·H$_2$O with LiF to give LiZnSO$_4$F is topotactic, and so it does not come as a surprise that this electrolyte-type layer is preserved in the final LiZnSO$_4$F phase. Now regarding the nature of the IL-LiZnSO$_4$F interactions, both XPS and NMR measurements suggest a different chemical environment in this layer, with a noticeable shift ($\delta = -1.5$ ppm) observed for the five peaks of the EMI cations in the ^{1}H NMR spectrum. Such a shift is most likely rooted in the proximity of the LiZnSO$_4$F surface, which additionally gives rise to relatively narrow lines for solid-state NMR spectra of ^{1}H (e.g. compared to the H$_2$O resonance in ZnSO$_4$·H$_2$O), thus indicating that the EMI-TFSI ions remain

quite mobile even if they are trapped onto the LiZnSO$_4$F-IL surface.

Turning to the enhanced lithium-ion conductivity, we can infer several possibilities such as 1) an increased LiF surface solubility, owing to the well-known fact that dielectric constants can easily be enhanced at truncated surfaces, and 2) an IL-driven enhanced disproportionate process that will facilitate the surface Li displacement. Although we cannot ascertain whether both effects take place simultaneously, we favor the latter as it is more consistent with the correlation in the NMR spectroscopy signal amplitude between the IL and LiF signals, which is also observed for samples purposely prepared with LiF deficiency. It is worth mentioning that such an ionic conductivity difference between ceramic- and ionic-liquid-made fluorosulfates is not general, as the ionic conductivity of LiFeSO$_4$F was found to be 10^{-11} S cm^{-1} irrespective of the synthesis route. Such different behavior between ZnSO$_4\cdot$H$_2$O and FeSO$_4\cdot$H$_2$O precursors with respect to ionic-liquid trapping is mostly related to differences in their chemistry, as already witnessed by the observed structural differences. Surface properties involving wettability, catalytic properties, or chemical reactivity are well known to be ruled out by the bulk crystal symmetry, with enhanced properties associated with the way that the surface is truncated along specific crystallographic directions. On that basis, the greater aptitude of the ZnSO$_4\cdot$H$_2$O phase towards capturing an ionic liquid monolayer at its surface is not a total surprise.

Overall, our LiZnSO$_4$F-IL can simply be viewed as a composite electrolyte formed of LiZnSO$_4$F grains surrounded by a conducting lithium-containing ionic liquid layer (e.g. electrolyte interface, Figure 2a), while the exact nature of the interface remains unclear. Future work will prioritize determining the exact nature of the ionic liquid/LiZnSO$_4$F surface by a variety of analytical techniques coupled with the development of chemical approaches to purposely graft ionic liquids on various surfaces. Although we have not yet elucidated the exact mechanism, we provide direct experimental evidence that ceramic powders "functionalized" with ionic liquids could provide a versatile route to turn disregarded Li-based ionic conductors into attractive solid electrolytes. This claim can only be supported by the recent achievement of extremely high conductivity in nanocomposite electrolytes based on LiF-functionalized titania plasticized with EMI-TFSI ionic liquid.[15] Although the presently achieved ionic conductivities in the range of 10^{-5} S cm^{-1} are still too low for developing practical solid-state lithium batteries, there is room for improvement owing to the rich ionic liquid chemistry.[14] We thus believe that composites of ceramics and ionic liquids as solid electrolytes could have a bright future in the field of energy storage.

Experimental Section

Synthesis: First, ZnSO$_4\cdot$H$_2$O monohydrate precursor was prepared by annealing commercial ZnSO$_4\cdot$7H$_2$O (Aldrich, 99%), either immersed in EMI-TFSI ionic liquid or in primary vacuum at 150°C for 1 h to remove excess structural water, washing the resulting powder with dichloromethane/ethyl acetate, and drying at 60°C. Then, LiZnSO$_4$F was synthesized through ionothermal synthesis by 1) mixing

ZnSO$_4\cdot$H$_2$O and LiF (in 1:1 molar ratio) in EMI-TFSI ionic liquid (3 mL) medium inside a Teflon-lined Parr bomb, 2) stirring the mixture for 5 min, and 3) heating the Parr bomb in an oven to 300°C for 5 h (heating rate 2°C min^{-1}). Upon cooling to ambient temperature, the reaction product was recovered by washing with dichloromethane, centrifuging, and drying the white powder at 60°C. Alternately, LiZnSO$_4$F can be synthesized by a solid-state route by mixing ZnSO$_4\cdot$H$_2$O with LiF (in 1:1 molar ratio) by ball-milling for 5 min, making a pellet using a uniaxial press (10 bar), heating the pellet inside a Teflon-lined Parr bomb reactor at 300°C for 30–40 h (heating rate 2°C min^{-1}) involving an autogeneous pressure (3 bar) before cooling it to room temperature to obtain the final product.

Characterization: X-ray diffraction patterns were collected on a Bruker D8-Advantage powder diffractometer using Cu-Kα radiation ($\lambda_1 = 1.54053$ Å, $\lambda_2 = 1.54431$ Å) equipped with a LynxEye detector (operating at 40 kV, 40 mA). Synchrotron powder diffraction data were collected in the Swiss–Norwegian Beam Lines (SNBL) at the European Synchrotron Radiation Facility (ESRF) in Grenoble, France. The sample was poured into a thin-walled glass capillary of 0.5 mm o.d. and measured at 295.0 K. The temperature was controlled with an Oxford Cryostream 700+ instrument. The data were collected using a MAR345 image plate detector at a sample-to-detector distances of 150, 250, and 400 mm, in order to combine high structural and angular resolutions, and a selected X-ray wavelength of $\lambda = 0.701277$ Å. The beam was slit to 300×300 μm. The capillary was oscillated by 30° during an exposure to the X-ray beam for 30 s. After the measurements at room temperature, the sample was studied in the 80–500 K range. For that it was cooled to 80 K and then heated from up to 500°C at a rate of 1 K min^{-1} while the diffraction patterns were collected. One pattern was recorded every 2 min (2 K steps), making a total of 212 patterns for the 80–500 K temperature scan. All of the obtained raw images were transformed into 1D powder patterns using the FIT2D program[16] and calibration measurements of the standard NIST LaB$_6$ sample. Uncertainties of the integrated intensities were calculated at each 2θ point by applying Poisson statistics to the intensity data and considering the geometry of the detector. The powder patterns were indexed using DICVOL,[17] and the complete structure was refined by Rietveld refinement using the FullProf program.[8] A total of 30 parameters has been used for the refinement in the following order: 1 for the scale, 3 for the cell parameters, 1 for the zero shift, 5 for the profile (pseudo-Voigt peak profile), 13 for the atomic positions, and finally 7 for the isotropic atomic displacement factors. Thermogravimetric analysis was conducted between 30 and ca. 800°C (heating rate 10°C min^{-1}, in air) using a Simultaneous Thermal Analyzer STA 449C Jupiter unit (Netzsch Inc). SEM microscopy images were obtained using an FEI Quanta 200 F field-emission scanning electron microscope (20 kV) operating under low vacuum to avoid any charging effects. Elemental analysis was performed at several spots to ensure homogeneous distribution of all elements. TEM microscopy images were obtained using an FEI Tecnai F20 S-Twin electron microscope (200 kV) on the powder sample deposited on a TEM holey (with carbon–copper) grid.

All NMR spectroscopy experiments were performed on a 7 T Bruker Avance NMR spectrometer (300 MHz for ^{1}H, 282 MHz for ^{19}F, and 117 MHz for ^{7}Li) using a 1.3 mm double-resonance probe for ^{1}H and ^{19}F operating at 60 kHz MAS and a 4 mm double-resonance probe for ^{7}Li operating at 14 kHz. Recycling delays for ^{1}H and ^{19}F were set to 120 s and four transients were recorded, using 150 and 200 kHz B^1 fields for excitation. The recycling delay was set to 1 s and 16 transients were recorded for ^{7}Li with a 1.1 μs long $\pi/12$ excitation pulse. The chemical shifts were referenced with 4-acetophenone at $\delta = -107$ ppm for ^{19}F and TMS at 0 ppm for ^{1}H. The peak relative intensities were calculated using the dmfit software.[18]

Conductivity measurements: LiZnSO$_4$F powder was pressed first by uniaxial press (10 bar) followed by isostatic press (2500 bar) to form a dense pellet 12 mm in diameter and 1–2 mm in thickness (75% theoretical density). Ionically blocking electrodes were made by

sputtering gold on both faces of the pellet. AC and DC conductivity studies were performed by employing (AC) impedance spectroscopy (200 kHz–10 mHz) and 1–2 V DC polarization, respectively. Varying the temperature from room temperature to 140°C, the conductivity data were recorded using a Bio-logic VMP3 instrument. Activation energies E_a for AC and DC conductivities were calculated by the Arrhenius relation $\log(\delta T) = \log(\delta_0 T_0) - E_a/k_B T$ (where δ = conductivity in $S\,cm^{-1}$, T = temperature, and k_B = Boltzman constant). Furthermore, polarization measurements (Li mobility) on a LiZn-SO$_4$F pellet were performed at 70°C by sandwiching the pellet between two sheets of PEO (soaked in 1M LiClO$_4$) and Li foils. By applying a constant voltage (25–100 mV), the DC current was recorded.

[1] N. Lewis, *MRS Bull.* **2007**, *32*, 808–820; J.-M. Tarascon, M. Armand, *Nature* **2001**, *414*, 359–367.

[2] M. Armand, J.-M. Tarascon, *Nature* **2008**, *451*, 652–657.

[3] A. K. Padhi, K. S. Nanjundaswamy, J. B. Goodenough, *J. Electrochem. Soc.* **1997**, *144*, 1188–1194.

[4] N. Recham, J.-N. Chotard, L. Dupont, C. Delacourt, W. Walker, M. Armand, J.-M. Tarascon, *Nat. Mater.* **2010**, *9*, 68–74.

[5] P. Barpanda, N. Recham, J.-N. Chotard, K. Djellab, W. Walker, M. Armand, J.-M. Tarascon, *J. Mater. Chem.* **2010**, *20*, 1659–1668; M. Ati, L. Dupont, N. Recham, J.-N. Chotard, W. T. Walker, C. Davoisne, P. Barpanda, V. Sarou-Kanian, M. Armand, J.-M. Tarascon, *Chem. Mater.* **2010**, *22*, 4062–4068; P. Barpanda, J.-N. Chotard, N. Recham, C. Delacourt, M. Ati, L. Dupont, M. Armand, J.-M. Tarascon, *Inorg. Chem.* **2010**, *49*, 7401–7413.

[6] B. V. R. Chowdari, G. V. Subba Rao, G. Y. H. Lee, *Solid State Ionics* **2000**, *136*, 1067–1075; J. Fu, *Solid State Ionics* **1997**, *96*, 195–200; J. B. Bates, N. J. Dudney, G. R. Gruzalski, R. A. Zuhr, A. Choudhury, C. F. Luck, J. D. Robertson, *Solid State Ionics* **1992**, *53*, 647–654.

[7] L. Sebastian, J. Gopalakrishnan, Y. Piffard, *J. Mater. Chem.* **2002**, *12*, 374–377.

[8] J. Rodriguez-Carvajal, *Physica B* **1993**, *192*, 55–69; S. Vogel, L. Ehm, K. Knorr, G. Braun, *Adv. X-Ray Anal.* **2002**, *45*, 31–42.

[9] P. G. Nagornyi, A. A. Kapshuk, N. V. Stus, N. S. Slobodyanik, A. N. Chernega, *Zh. Neorg. Khim.* **1991**, *36*, 2766–2768.

[10] K. Fujii, Y. Soejima, Y. Kyoshoin, S. Fukuda, R. Kanzaki, Y. Umebayashi, T. Yamaguchi, S. Ishiguro, T. Takamuku, *J. Phys. Chem. B* **2008**, *112*, 4329–4336.

[11] J.-C. Lasségues, J. Grondin, C. Aupetit, P. Johansson, *J. Phys. Chem. A* **2009**, *113*, 305–314.

[12] B. Kang, G. Ceder, *Nature* **2009**, *458*, 190–193.

[13] S. S. Moganty, N. Jayaprakash, J. L. Nugent, J. Shen, L. A. Archer, *Angew. Chem.* **2010**, *122*, 9344–9347; *Angew. Chem. Int. Ed.* **2010**, *49*, 9158–9161.

[14] M. Armand, F. Endres, D. R. MacFarlane, H. Ohno, B. Scrosati, *Nat. Mater.* **2009**, *8*, 621–629.

[15] V. Di Noto, M. Piga, F. Bertasi, E. Negro, Abstract in Ionic Liquids for Electrochemical Devices, Rome 9–11 Jun 2010.

[16] A. P. Hammersley, S. O. Svensson, M. Hanfland, A. N. Fitch, D. Häusermann, *High Pressure Res.* **1996**, *14*, 235–248.

[17] A. Boutlif, D. Louer, *J. Appl. Cryst.* **2004**, *37*, 724–731.

[18] D. Massiot, F. Fayon, M. Capron, I. King, S. Le Calvé, B. Alonso, J. O. Durand, B. Bujoli, Z. Gan, G. Hoatson, *Magn. Reson. Chem.* **2002**, *40*, 70–76.